Journal of Engineering and Technological Sciences

Design of a Novel Efficient High-Gain Ultra-Wide-Band Slotted H-Shaped Printed 2×1 Array Antenna for Millimeter-Wave Applications with Improvement of Bandwidth and Gain via the Feed Line and Elliptical Edges

Tibermacine Badreddine^{1,*}, Hamaizia Zahra² & Guesbaya Tahar³

- ¹Departement of Electrical Engineering, Laboratory of Metallic and Semiconducting Materials (LMSM), Biskra University, 37 Salah Bey Road, BP 07000, Biskra State, Algeria
- ²Departement of Electrical Engineering, Biskra University, Pont Blonc 100 Logements Bloc 5, BP 23000, Annaba State, Algeria

Corresponding author: tiberbadreddine@gmail.com

Abstract

This paper describes design procedure of a high-performance miniaturized antenna with an array configuration, which contributes to enhancing the communication system's performance. The basic antenna features a compact size (6 x 6) mm2, and its single element is an H-shaped slotted patch printed on the top side of a Rogers RT5880 substrate, with a relative permittivity and thickness of 2.2 and 0.3 mm, respectively. The edge-to-edge distance of the 2×1 array antenna is 9×14 mm2, and the isolation between its radiation elements is 4.5 mm. To increase the capabilities of the antenna in terms of gain and bandwidth, we proceeded to use the 2×1 array configuration and then optimized the model via either the width of the feed line or the elliptical edges of the patch. The miniaturized array antenna achieved a peak gain of 12.56 dB, a directivity of 13.11 dBi, and a return loss of -47.52 dB at a resonance frequency of 91.5 GHz, with a radiation efficiency of more than 91% over an operating bandwidth of 15.83 GHz, ranging from 79.7 GHz to 95.6 GHz. The design and simulation results of the proposed antenna were obtained using the CST Studio software.

Keywords: array antenna; CST studio; millimeter wave; miniature; ultra-wide band; slots.

Introduction

As a core device for wireless technology, many studies have been conducted on antenna systems, especially micro strip patch antennas (MPAs), which are the most recent development in the field of antennas and have been integrated into a variety of applications (including radio-frequency identification (RFID) [1-2], active antenna unit of a 5G base station[3],and multiple-input multiple-output (MIMO) systems [4,5]) because of their obvious benefits of flat shape, low cost, easy integration, and fabrication. On the other hand, MPAs have a number of disadvantages too, the most significant of which are low gain, limited bandwidth, and high feed network losses. As a result, numerous antenna researchers have made significant attempts to alleviate these limitations, for example improving the bandwidth by increasing the thickness of the substrate [6] or using stubs [7], a negative capacitor/inductor [8], a non-Foster matching circuit [9-14], a U-E-H shaped patch [15], an L-shaped antenna with U-shaped slot [16], defected ground structures (DGS) [17], magneto-dielectric substrates [18-20], electromagnetic band-gap (EBG) structures [21,22], meta-material resonators [23-25], fractal geometries [26-28], and cavity backing [29,30]. While gain improvement is possible with dielectric-loaded exponentially tapered slot antennas [31] and substrate-integrated waveguides (SIW) [32], this is also possible with the use of array antennas, as they offer the advantage of high gain [33-35]. However, the need for small, compact array antennas and the shift to millimeter- and terahertz-wave applications have led to a big

Copyright ©2023 Published by IRCS - ITB ISSN: 2337-5779

J. Eng. Technol. Sci. Vol. 55, No. 1, 2023, 60-78 DOI: 10.5614/j.eng.technol.sci.2023.55.1.7

³Departement of Electrical Engineering, Biskra University, 20 El-Allia Road, BP 07000, Biskra State, Algeria

DOI: 10.5614/j.eng.technol.sci.2023.55.1.7

degradation in the performance of the array, resulting from strong mutual coupling between radiating elements. To overcome this, a number of mutual-coupling suppression (decoupling) techniques have been applied to improve the performance of the antenna's parameters, including the use of electromagnetic band-gap (EBG) structures [36-41], meta-materials (MTM) [42-48] and on-chip antennas based on meta-material, meta-surface, and substrate integrated waveguide principles for millimeter- and terahertz-wave integrated circuits and systems. On-chip antennas are suitable for tablet computers, cell phones, headsets, and WiFi and WLAN routers.

The above-mentioned technologies introduced in on-chip antennas, yield significantly improved impedance match, bandwidth, gain, and radiation efficiency [49-53]. These techniques have been introduced to effectively limit mutual coupling between adjacent radiation elements that can otherwise degrade the array's radiation gain and pattern. EBG meta-surface and meta-material based antenna techniques provide structural simplicity, which lowers manufacturing costs. Additionally, a very broad frequency coverage with excellent performance can be attained. The ever-increasing demand for wireless applications that deliver high-quality content to a large number of users simultaneously has resulted in a massive increase in data volume, which has resulted in a shortage of spectrum in the microwave band, causing networks to become congested. To address this issue, researchers have moved to millimeter wave (30 to 300 GHz) usage, where we find some appealing applications, for example, wireless digital data transfer allocated around 60 GHz between a high-definition TV (HDTV) and a DVD player of uncompressed high-definition video, autonomous robots, and back hauling allocated around 80 GHz; and motion sensing at 100 GHz.

The mm-wave choice is appropriate for the main reason that mm-wave systems have larger available bandwidth as compared to other communication frequencies below 10 GHz because of a metric called the fractional bandwidth (for example, designing a system that occupies 5% of the operating frequency means having 5 GHz of available bandwidth at 100 GHz) and it is well-known that the larger bandwidth enhances the channel capacity. On the other hand, because radio signals at millimeter-wave frequencies attenuate significantly with distance for many applications, it is vital to pick an appropriate frequency band with the least attenuation to obtain maximum distance and minimize attenuation. Due to their lower attenuation, the bands between 10 to 40 and 70 to 100 GHz are currently the most commonly used [54,55]. In general, the losses caused by electromagnetic wave atmospheric absorption at higher frequencies remain constraints for mm-wave applications. Therefore, antenna arrays come as a solution to achieve higher gain and efficiency. This study focused on two main axes: the influence of the array configuration on gain and efficiency improvement, and how to obtain a wider bandwidth.

The Approach Used in the Presented Work

Starting from the fact that we aimed to develop an antenna that meets criteria defined beforehand, i.e., higher gain and wider bandwidth, an accurate plan was drawn up (Figure 1) that clarified the steps to be taken to achieve the desired characteristics. In the first stage, the goal was to design a basic antenna (with a single patch). The desired results obtained after optimization were then used in the next stage.

The first stage started with the choice of the substrate material, because it is of great importance in the search for an efficient antenna operating at high frequencies. Before determining the initial antenna geometry, to be operated at a frequency chosen in advance, using established formulas derived from transmission line model analysis and then optimizing the design to achieve the desired results, it is necessary to mention that we started by designing an antenna with a square patch and then made changes in the shape to improve the characteristics of the antenna, i.e., bandwidth and gain.

The second step (2×1 array antenna) was based on the findings of the previous stage, and because we wanted to optimize the bandwidth and gain values as much as possible, two distinct methods of antenna bandwidth optimization were adopted. The basis of the first method was to adjust the main feed line width. The second approach involved varying the radius of the ellipse positioned on the patch's sides and then comparing the outcomes in terms of bandwidth, gain, and radiation properties in order to find the best results. After we got the desired results, the last step was to create the antenna's design according to these results, i.e., the antenna design proposed in this work. The work was based on the use of the CST software for calculation and design during both stages. The calculation procedure was done using transmission line model analysis.

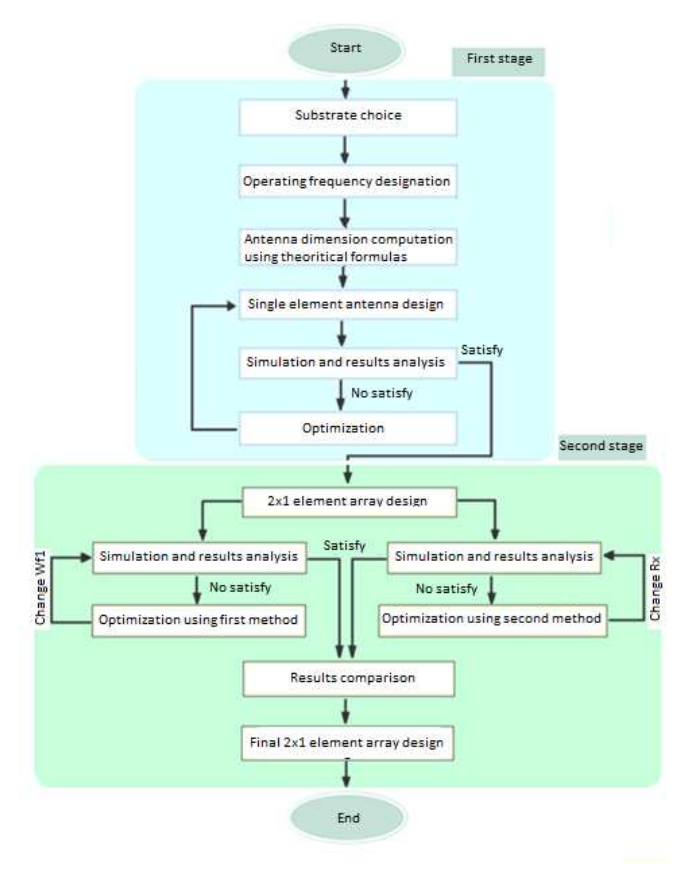


Figure 1 Methodology of the present work.

Results and Discussion

Several methods have been applied for the analysis of micro-strip antennas, which can be classified into two categories: approximate methods and rigorous methods (full-wave). The first ones are based on simplifying the assumptions, because of which they have limitations and provide less precise solutions. They are generally used for modeling single-element antennas due to the difficulty encountered in modeling the coupling between several elements. They do, however, provide a good physical overview with very little computation time. The rigorous methods take into consideration all the important wave mechanisms and rely heavily on the use of efficient digital algorithms. The rigorous methods are very precise when applied properly and can be used for modeling a variety of antennas, including array antennas. These methods tend to be more complex and provide less of a physical overview. Often, they require more calculations, which means higher calculation time. As approximate methods, we have the transmission line model and the cavity model. The rigorous methods include finite element methods, the finite difference method (FDTD), the transmission line matrix method (TLM), and the method of movements. In this work, the calculation procedure was done using transmission line model analysis.

Antenna Modeling

To understand how an antenna works, it is important to look at its physical components, the parameters that describe its behavior, and the model used to evaluate the antenna. The patch is usually made of a conductive material, such as copper or gold, and is generally photo-etched onto the insulating substrate. It can have many shapes, such as dipole, monopole square, triangular, circular, rectangular, or other different complicated shapes, but rectangular and circular are most commonly used, because they are very easy to analyze and manufacture. Various substrate materials can be employed, including ceramic, ferromagnetic, semiconductor, and synthetic materials. The substrate serves both as a dielectric medium for etching the circuits and a mechanical support for

DOI: 10.5614/j.eng.technol.sci.2023.55.1.7

the construction. Low dielectric losses are often employed to increase antenna performance, and low relative permittivity substrates are often used to improve the radiation while lowering the losses. The printed antenna is excited. This means that energy is supplied to the patch so that we can directly influence its radiation and modify it to attain high performance. To excite the antenna, two techniques can be used: the contacting feed technique (the power is transmitted directly to the patch by a coaxial probe or micro-strip line) and the non-contacting feed technique (the power is transmitted to the patch via electromagnetic coupling, whether proximity coupling or aperture coupling).

Resulting Designs

Antenna With a Single Patch

As can be seen in Figure 2(a), the antenna was formed by two pieces of copper with 0.035 mm of thickness, representing the patch and the ground plane, separated by Rogers RT5880 material as the substrate, whose characteristics are represented in thickness (h), loss tangent, and permittivity, which were 0.3 mm, 0.0009, and 2.2, respectively. The patch contained a small horizontal stub in each corner; see Figure 2(b). The lateral edges are semi-ellipse-shaped, playing a major role in the antenna performance.

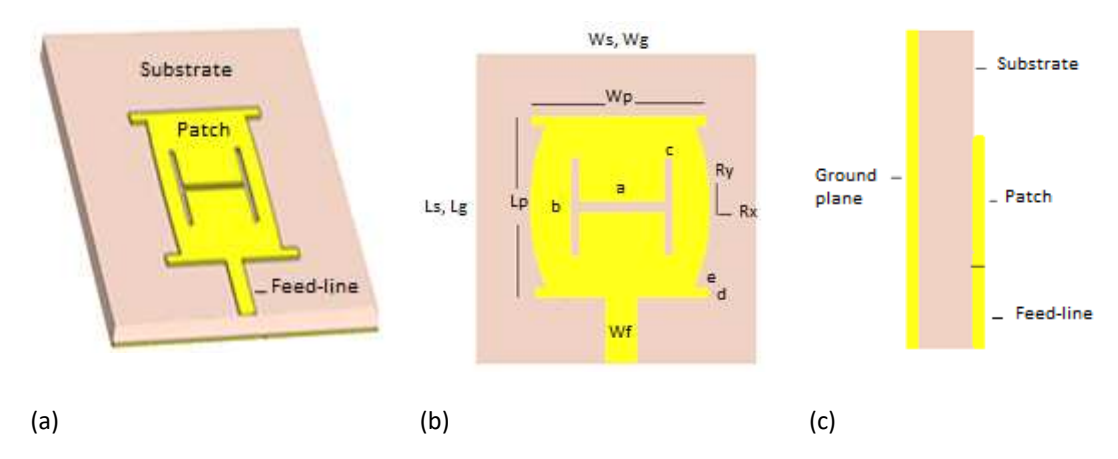


Figure 2 Basic antenna: (a) 3D shape, (b) geometry dimensions, (c) side view.

A 50-Ohm feed line technique was employed to achieve impedance matching between the antenna and the feed line; as can be seen above, the antenna was H-shaped slotted. The employment of this slotting technique allows for multiband behavior. To design the target antenna, we first built a basic antenna, whose patch was employed as a fundamental element in the final antenna design. Initially, we assumed that the patch was rectangular in shape. The dimensions were theoretically computed to a frequency of 80 GHz by referring to Eqs. (1) to (5) stated below. Rectangular and square patch antennas have the same calculation procedure for the size (L x W), except that for the square patch, the width is neglected. As a result, the size of the square patch will be (L x L) rather than (L x W) as it is for the rectangular patch. The width was computed using the formula:

$$W = C / 2fr \left[(\varepsilon r + 1) / 2 \right] \frac{1}{2}$$
 (1)

c =velocity of light in air

fr = operating frequency

εr = dielectric permittivity

The length was computed using the formulas:

$$\epsilon \operatorname{reff} = (\epsilon r + 1) / 2 + [(\epsilon r - 1) / 2] (1 + 12h / W)^{-1}/2$$
 (2)

ereff =effective dielectric constant
h =height of substrate

Leff =
$$C/2$$
fr (reff) $\frac{1}{2}$ (3)

$$\Delta L= 0.412h [(W/h+0.264) (\epsilon reff+0.3)]/[(\epsilon reff-0.258) (W/h+0.8)]$$
 (4)

$$L = Leff - (2 \Delta L) \tag{5}$$

Leff = effective length

ΔL =length extension

L = length

The calculation procedure was done using the transmission line model analysis mentioned above. The patch length and width were found to be 1 mm and 1.5 mm, respectively, but because the antenna had to be optimized to meet the desired performance characteristics(represented in gain, bandwidth, and frequency of resonance), they were then adjusted to Lp = 3 mm and Wp = 3 mm. All the details regarding the antenna model dimensions with a single patch are given in Table 1. The antenna was square-shaped (6 x 6 mm²), while the patch was not because of the elliptic-shaped sides, but we could use the existing theoretical formulas to approximate the initial dimensions of the antenna at the desired frequency. We also note for the ellipses that the vertical radius Ry stayed fixed and was substantially larger than the horizontal radius Rx, in the order of 1/100 millimeters. Rx has a great and direct influence on the antenna parameters, and it gave good results, especially in the range of 0.01 to 0.05 mm (see the discussion part for the second stage). The same goes for the width Wf of the feed line, which also has a remarkable impact on the antenna behavior, like that of the elliptical-shaped radius.

Value (mm) **Parameter Parameter** Value (mm) Ws 6 Rx 0.05 Wg 6 Ry 1.4 6 1.5 Ls а 6 1.5 Lg b Wp 3 С 0.1 3 d 0.17 Lp

е

0.38

0.3

0.36

1.1

Table 1 Single element antenna dimensions.

Second Stage: 2 x 1 Array Antenna Design

Wf

Lf

The second stage was reserved for designing the proposed antenna; Figure 3 depicts the geometry of this antenna. As shown in Figures 3(a) and (b), the design of the antenna was fundamentally based on the previous design, with the exception that the feeding network underwent a small modification in the feed line dimensions corresponding to the patches, and inset feeding was used at each patch to feed the two elements to lower the input impedance, which provides higher antenna efficiency; a corporate feed line is connected with the network, which serves as a T-junction power divider to create the 2 x 1 array configuration. The feed lines' dimensions were set to maximize the matching between the source and the antenna represented by the two patches. Meanwhile, the substrate and ground plane dimensions as well as the substrate thickness were kept without modification. The antenna patches were positioned at a well-determined and precise distance (S) of separation in order to get good insulation. The size of the new model was 14 x 9 mm2, still retaining the advantage of miniaturization. Also note the presence of notches with length and width measurements of 0.3mm and 0.02mm, respectively, which are due to the use of the inset-feeding technique.

The aim of this was to perfectly match the impedance of the patch with the feed line. The patch was not modified; it still had the H-shaped slot and the little stubs; we merely multiplied this patch to get the array configuration (Table 2 provides the geometry of this design). When we look at, for example, the substrate and ground plane width dimensions (Ws and Wg) in Table 2, we see that, in reality, it is as if two antennas from the previous stage (single-patch antenna) are placed in a cascade, so that the patches are distanced by 4.5 mm. The new feature in this stage was that we used the inset-feeding technique (notches) in addition to the feed network.

Geometrically, the 2 x 1 element array antenna became rectangular in shape, while the symmetry was preserved, as a symmetrical structure produces better results and reduces simulation time.

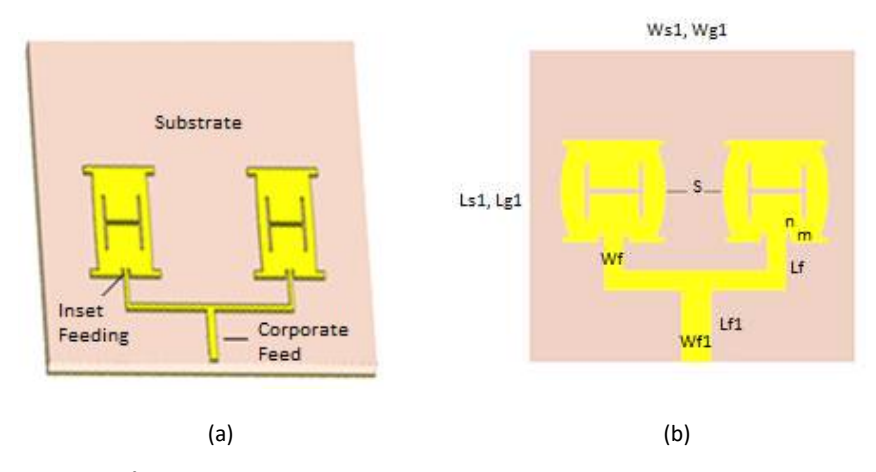


Figure 3 Proposed antenna:(a) 3D shape, (b) geometry dimensions.

Parameters Values (Mm) Values (Mm) **Parameters** Ws Wf 14 0.15 Wg 14 Lf 0.77 Ls 9 S 4.5 9 0.02 Lg m Wf1 0.33 0.3 n Lf 1 1.4 h 0.3

 Table 2
 Suggested antenna dimensions.

Antenna Characteristics Results

Antenna with a Single Patch

The antenna characteristics are primarily determined by the patch geometry, the excitation technique, the substrate thickness, and the dielectric constant, which are all considered critical for monitoring the antenna's behavior and improving the performance. In this work, we first optimized the basic antenna (with a single patch), the results of which were then used to design the target antenna (with 2 x 1 patches). Figure 4 depicts the variation in the S-parameter as a function of frequency change. The reflection coefficient (return loss) is the rest of the power that does not radiate, which allows us to know the quality of adaptation of the antenna, or an antenna with impedance Zant, connected to the source by a characteristic impedance line Zc. The reflection coefficient is:

$$S11 = (Zant - Zc) / (Zant - Zc)$$
(6)

Zant and Zc represent the antenna impedance and characteristic impedance, respectively. The reflection coefficient depends on the value of S11 and should be less than -10 dB in magnitude; as is expressed below, the single patch antenna is triple-band. It resonates at three frequencies: 61.3 GHz, 73.25 GHz, and 87.7 GHz, which correspond to bandwidths of 1.66 GHz, 6.13 GHz, and 6.47 GHz, respectively. The achieved reflection coefficients at these frequencies were -20 dB, -17 dB, and -27 dB, respectively. Table 4 describes these results well. The gain is the ability of the antenna to radiate less or more in any direction (θ, ϕ) compared to a theoretical antenna called isotropic non-existent, which radiates in all directions in reality.

$$G(\theta, \phi) = 4\pi p(\theta, \phi) / PA \tag{7}$$

PA =power of the antenna

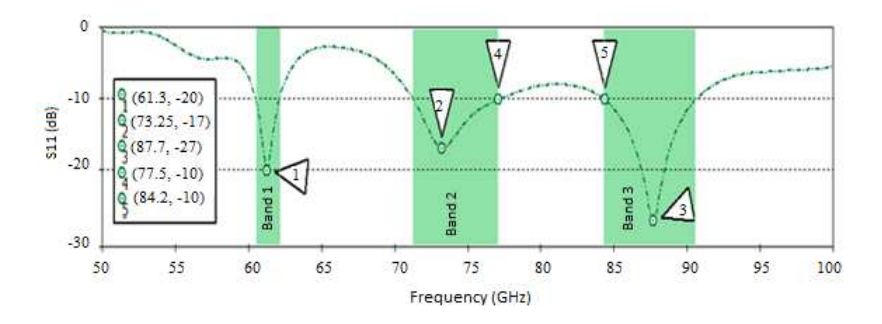


Figure 4 Reflection coefficient of the single-patch antenna.

Figure 5 shows the 2D radiation pattern plot of the realized gain for the antenna with a single patch at frequencies of 61.3 GHz, 73.25 GHz, and 87.7 GHz. It demonstrates that this antenna at a resonant frequency of 87.7 GHz generated a low side lobe level of -3.9 dB, a half power bandwidth (HPBW) or angular width (3 dB) of 45.3°, and a main lobe magnitude of 7.95 dB. The best attributes of the other centers of frequency were as follows: at 61.3 GHz in the H-plane, the antenna had a low side lobe level (SLL) of 12.6 dB, an angular width (3 dB) of 48°, an angular width (3 dB) of 42.6°, and a main lobe magnitude (MLM) of 6.05 dB. At 73.25 GHz in the E-plane, the antenna had a low side lobe level of -12.4 dB, an angular width (3 dB) of 64.8°, and a main lobe magnitude of 1.64 dB. The directivity indicates in which directions the power density was better or worse than that of the isotropic antenna.

$$D(\theta, \phi) = 4\pi p(\theta, \phi) / PR$$
 (8)

P (θ , ϕ) =radiated power per unit of solid angle (θ , φ)

PR =total radiated power

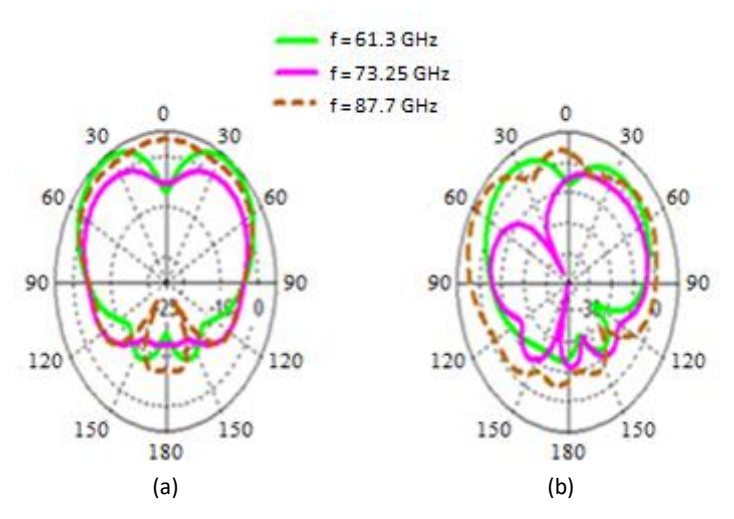


Figure 5 Realized gain radiation for the single antenna patch: (a) H-magnetic field plane, (b) E-electric field plane.

Figure 6 (a), (b), and (c) represent three-dimensional plots of the directivity radiation of the single-patch antenna at 61.3 GHz, 73.25 GHz, and 87.7 GHz. We opted to show the radiation characteristics of directivity at all the frequency spots to illustrate the place with maximum directivity (8.67 dBi at 87.7 GHz, as opposed to 6.74 dBi and 7.05 dBi at 61.3 GHz and 73.25 GHz, respectively). The antenna radiates in the upper mid-sphere with a direction of 0° in the H-plane and 57° in the E-plane; this performance also concerns certain other characteristics.

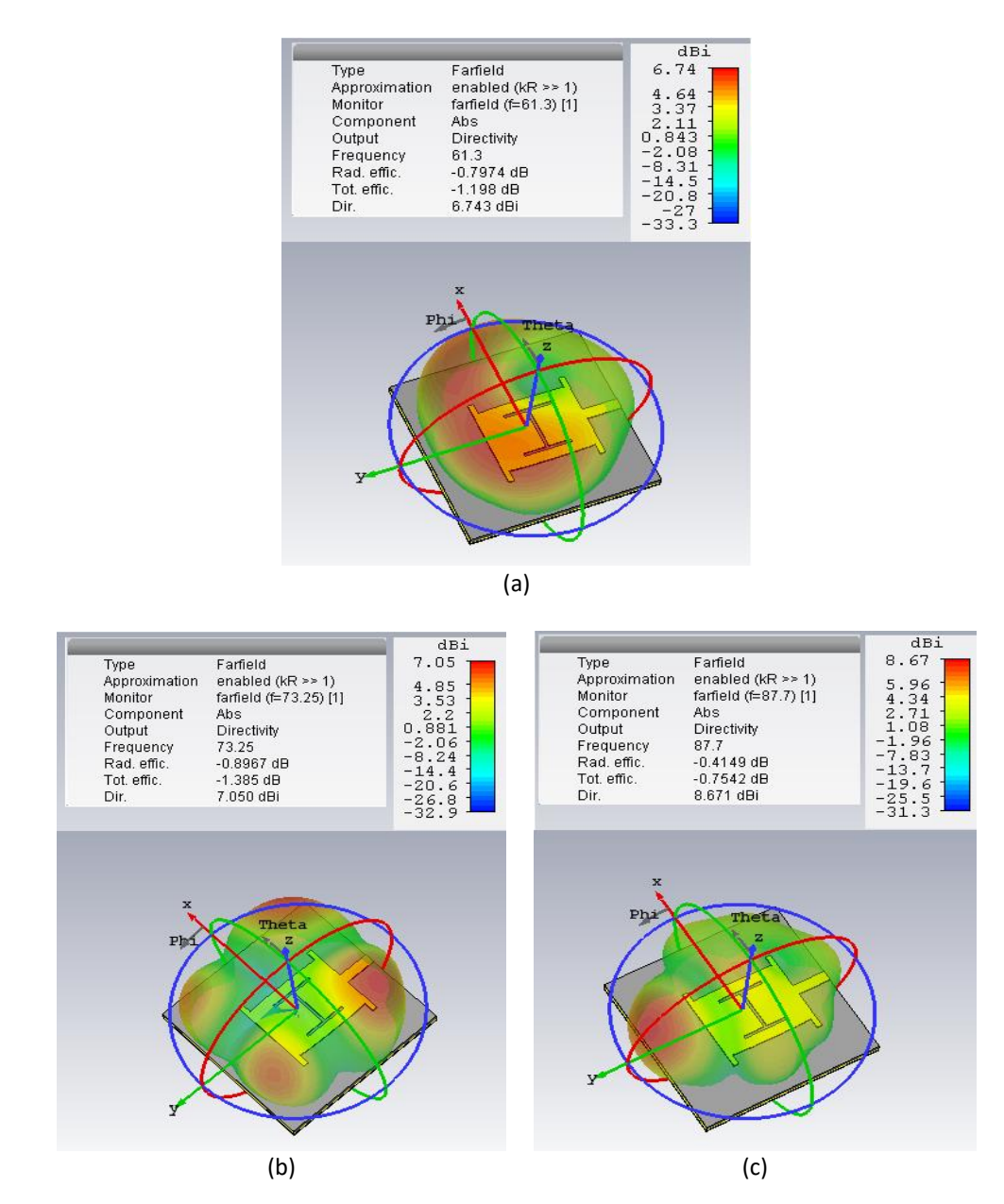


Figure 6 3D directivity radiation for the single antenna at: (a) 61.3 GHz, (b) 73.25 GHz, (c) 87.7 GHZ.

Figure 7 presents a comparative showing of gain and efficiency as a function of frequency change. As shown below, there is an approximate proportionality between the two curves at certain frequency ranges. To validate this, here is a summary of the results extracted from the two curves: for the frequency band (61.3 GHz), the average radiation efficiency and realized gain were about 82.3% and 5.55 dB, respectively; the maximum realized gain was 5.94 dB and the maximum directivity was 7.5 dBi, both at 62.25 GHz. For the frequency band (73.25 GHz), the average radiation efficiency and realized gain were about 76.5% and 5.5 dB, respectively, with a maximum realized gain of 7 dB and a maximum directivity of 8.6 dBi, both at 77.3 GHz. For the frequency band (87.7 GHz), the average radiation efficiency and realized gain were about 85% and 7.35 dB, respectively; it had a maximum realized gain of 8.84 dB and a maximum directivity of 9.6 dBi, both at 90 GHz, and a maximum efficiency of 91% at 86.6 GHz. The antenna with a single patch gave good results in terms of gain (8.84 dB), directivity (9.6 dBi), efficiency (91%), and coefficient of reflection (-27 dB) in the frequency band of 87.7 GHz. Table 4 illustrates these results.

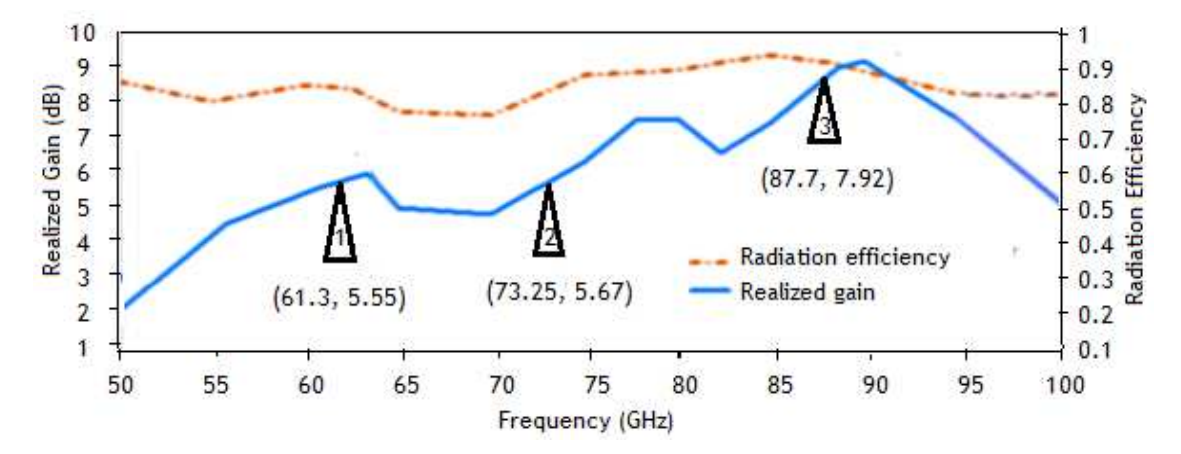


Figure 7 Radiation efficiency and realized gain for the single antenna.

Array Antenna

As is well known, bandwidth and reflection coefficient values play an important role in determining the efficiency of any antenna device. They depend on several parameters, such as frequency, patch shape, characteristics of the substrate, and other post-processing parameters. Several techniques allow the enhancement of antenna performance in terms of bandwidth, as shown in Figure 8 below.

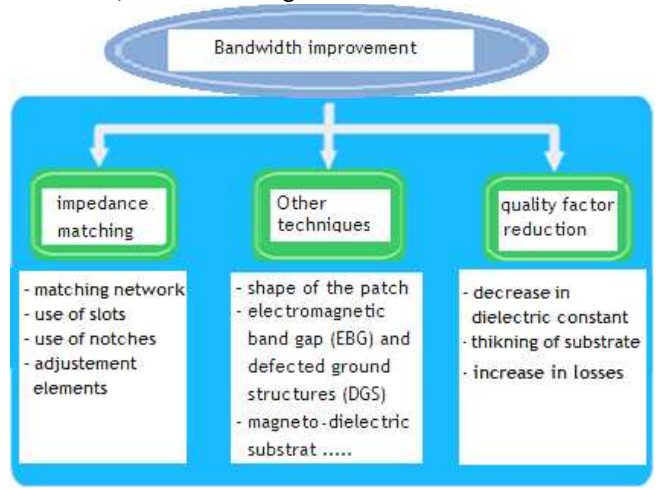


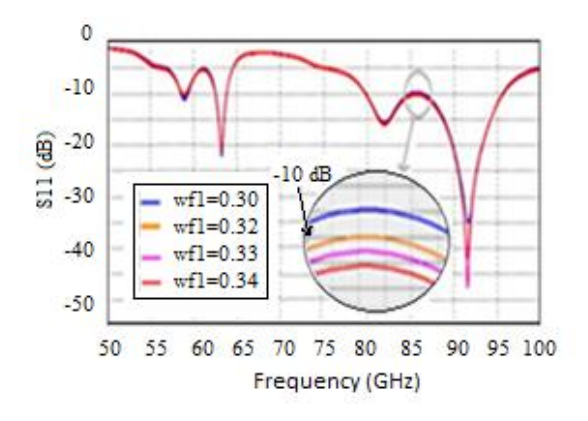
Figure 8 Bandwidth improvement.

In this project, we employed the approach of changing the shape of the patch. During the design process, it was discovered that two elements had an impact on performance: the horizontal radius (Rx) of the elliptical shapes and the feeding line width (Wf1). Figures 9 and 10 show the impact on bandwidth and reflection coefficient as a result of these two factors. Thus, we tried two ways to improve the antenna's performance: the first method used Rx = 0.05 and Wf1 = variable and the second method used Rx = variable and Rx = 0.33. For both methods, a noticeable improvement in terms of bandwidth occurred. We note that we chose four positions either for Rx or for Rx = 0.05 must be describe well the behavior of the antenna in terms of bandwidth: the antenna impedance bandwidth begins to change and widen from Rx = 0.03 mm and Rx = 0.03 mm for the first and second methods, respectively; at Rx = 0.03 mm and Rx = 0.05 mm, it achieved a wider bandwidth of 15.83 GHz, ranging from 79.7 to 95.6 GHz (S-parameter less than -10 dB) and became a dual band instead of a triple band; for the second method, particularly at Rx = 0.07 mm, the lowest reflection coefficient of the antenna was -65 dB.

When comparing the two methods, we can see that the antenna kept the same frequency band intervals with approximately the same resonant frequencies: 63.2 GHz and 91.5 GHz for the second stage and 61.3 GHz, 73.25 GHz, and 87.7 GHz for the first stage, so there was no notable shift in frequency bands or even in resonant

frequencies. The only difference was in the reflection coefficient. For the second method, the antenna had better results in terms of reflection coefficient (-65 dB) for Rx = 0.07 mm than for Rx = 0.05 mm (-47.52 dB), but a relative decrease in realized gain occurred (see Figure 11), 12.50 dB for Rx = 0.07 mm, and 12.55 dB for Rx = 0.05 mm. It was in this observation that the choice of the geometry of the antenna rested. Based on the findings, we conclude that by adjusting or properly selecting the antenna shape, the bandwidth and reflection coefficient can be reduced and increased.

We also note that any change in Rx or Wf1 leads to a small shift in resonant frequency, but it is not significant. Because we are interested in the gain value, Rx and Wf1 for the design were set to 0.05 mm and 0.33 mm, respectively, as can be seen in Figure 11. By comparing the two methods (see Figure 11), we aimed to maximize the gain and efficiency as much as possible, even if the improvement was a little smaller than expected. Figure 12 depicts the curve produced by the variation of gain and efficiency as a function of frequency. The finalized design of the proposed antenna is deemed to have promising operating characteristics. The realized gain reached a high value of 12.56 dB, as did the efficiency at 94% (Figure 12) and the maximum directivity at 13.11 dBi (Figure 13), all of which were reached at a resonant frequency of 91.5 GHz, which is part of the well-known frequency range between 70 and 100 GHz. Referring to Figure 9 or Figure 10, we note that the transition between both stages led to the exclusion of a frequency band (Figure 4, points 4 and 5), so the antenna became dual-band instead of triple-band. The resulting frequency bands were those corresponding to resonant frequencies of 63.2 GHz and 91.5 GHz.



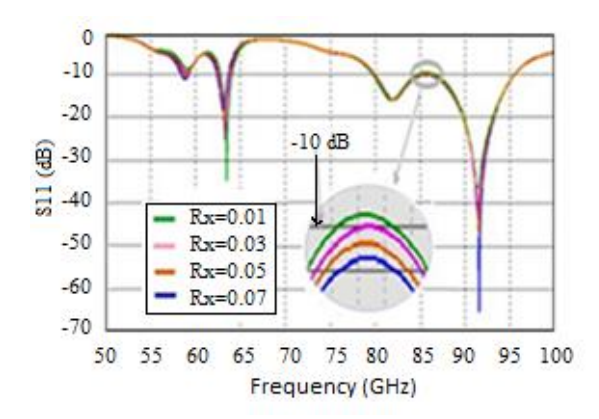


Figure 9 Reflection coefficient for the first method.

Figure 10 Reflection coefficient for the second method.

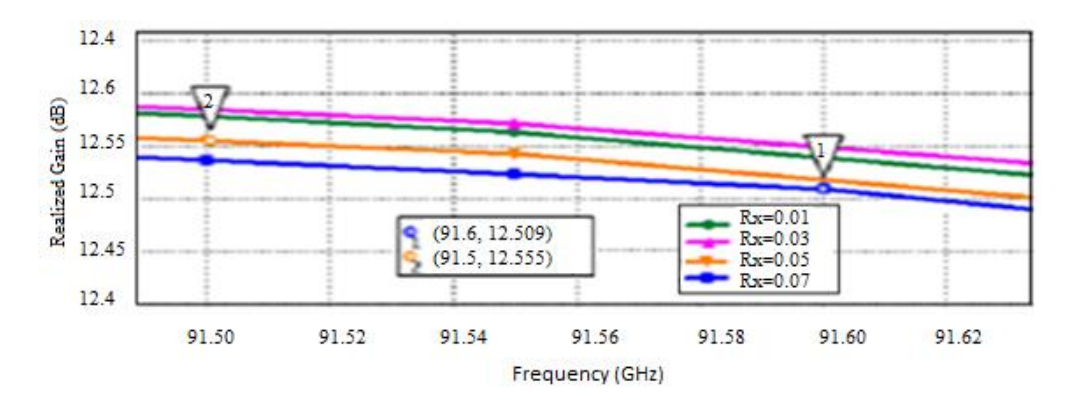


Figure 11 Gain comparison for the second method.

In Figure 12, we can distinguish these two frequency bands. At the frequency band (63.2 GHz), the antenna had a reflection coefficient of -21.18 dB; the average values of realized gain and radiation efficiency over this band were about 7.4 dB and 89%, respectively; the antenna achieved a maximum gain of 7.80 dB and a maximum directivity of 8.75 dBi at 62.5 GHz. At the frequency band (91.5 GHz), it has a reflection coefficient of -47.52 dB; the average realized gain and radiation efficiency over this band were 9 dB and 92%, respectively. It was in this

frequency band that the antenna achieved its maximum gain of 12.56 dB and its maximum directivity of 13.11 dBi, exactly at the resonant frequency of 91.5 GHz. When compared to the 63.2 GHz frequency band, the antenna's strong performance at 91.5 GHz is remarkable.

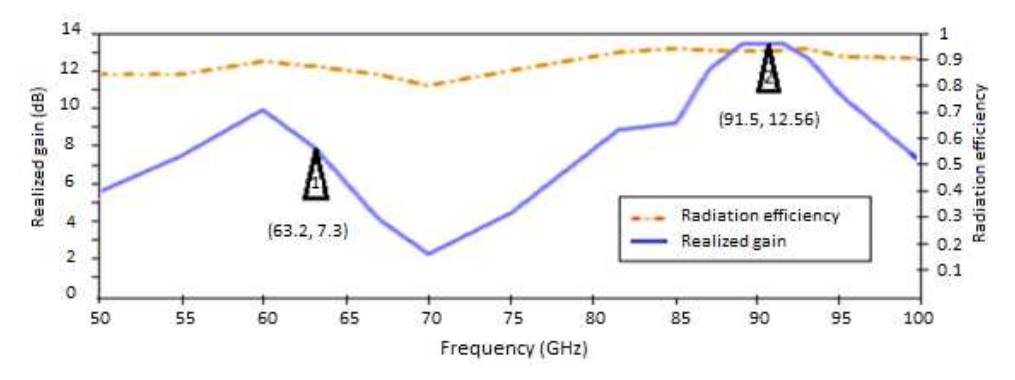


Figure 12 Realized gain and radiation efficiency.

The 2D radiation pattern plot of the proposed antenna at resonant frequencies of 63.2 GHz and 91.5 GHz is shown in Figure 13. What we can deduce from this figure is that the proposed antenna has excellent characteristics at 91.5 GHz, including a half power bandwidth (HPBW) or angular width (3 dB) of 21.6° in the Hplane and a main lobe magnitude (MLM) of 12.6 dB in the E-plane. As shown in Table 3, the resonant frequency of 63.2 GHz has a high side lobe level (SLL) of -0.6 dB and a main lobe magnitude (MLM) of 7.24 dB in the Eplane, but it is more directive in the H-plane with a half power bandwidth (HPBW) of 29.8° and has a low side lobe level (SLL) of -4 dB. The comparison excludes the main lobe direction (MLD). Figure 14 depicts a threedimensional plot of the proposed antenna's directivity radiation at 63.2 GHz and 91.5 GHz. The antenna radiated in the upper mid-sphere, roughly in the direction of the z-axis, and it recorded a high directivity at 91.5 GHz, 13.11 dBi, as shown in Figure 14 (b). With an angular width of 21.6° and 34.2° in the H-plane and E-plane, respectively, it was more directive than the one in the first stage at 87.7 GHz, which had a directivity of approximately 8,67 dBi, and an angular width (3 dB) of 45.3° in the E-plane, as shown in Table 3. It can also be seen from Table 3 that the final obtained antenna featured very strong radiation characteristics at 91.5 GHz, including high directivity (Figure 14) of 21.6° in the H-plane, a main lobe magnitude of 12.6 dB and a low side lobe level of -6 dB in the E-plane. All of the collected antenna parameter findings, including the radiation characteristics, are shown in Table 4.

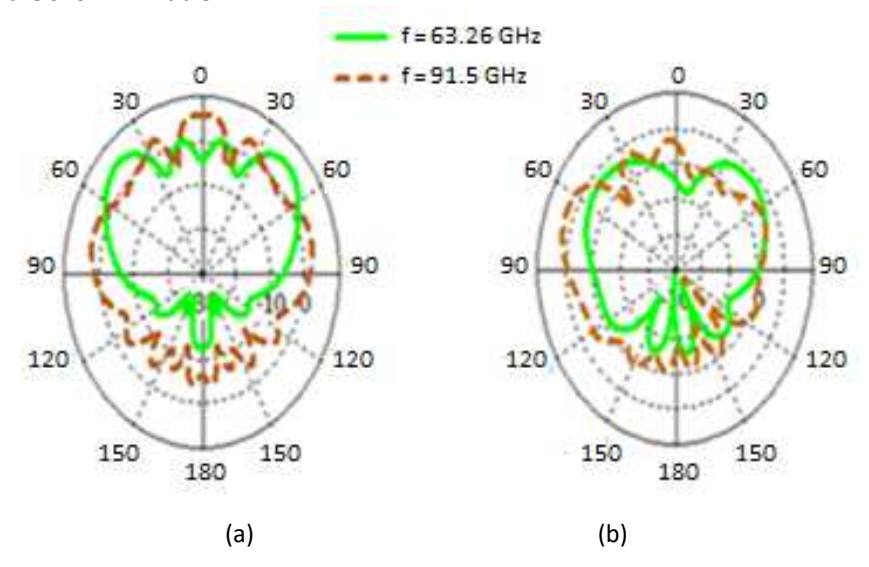


Figure 13 Realized gain radiation: (a) H-magnetic field plane, (b) E-electric field plane.

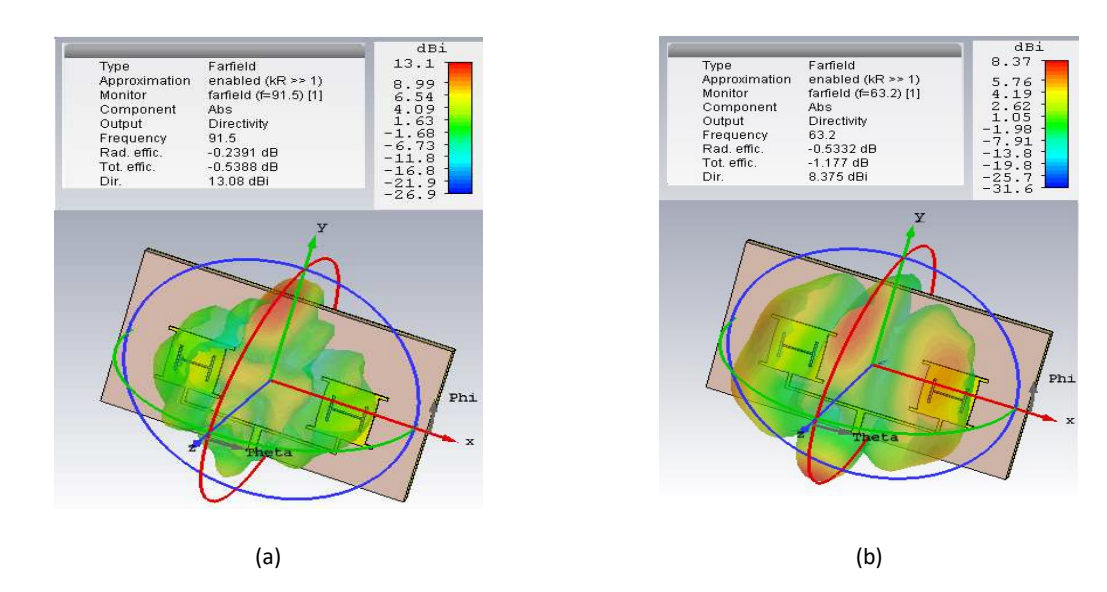


Figure 14 3D directivity radiation at: (a) 63.2 GHz, (b) 91.5 GHz.

 Table 3
 Radiation results throughout both stages.

Design	Resonant Freq (GHz)	Plane	MLM (dB)	MLD (Degree)	HPBW (Degree)	SLL (dB)
Single	61.3	E	6.05	35	42.6	-2.4
patch		Н	5.45	36	48	-12.6
	73.25	E	-1.08	51	96.4	-2.2
		Н	1.64	42	64.8	-12.4
	87.7	Е	8.71	57	45.3	-3.9
		Н	4.14	0	132.9	-8.4
2x1	63.2	Е	8.42	47	41.4	-0.6
Element		Н	4.62	46	29.8	-4.5
array	91.5	E	12.6	67	34.2	-6
		Н	5.73	4	21.6	-2.6

The fact that such a small antenna (14 mm x 9 mm) can achieve such a high directivity value is a significant advantage, and it addresses an obstacle for researchers, because few antenna designs possessing such a compact size can achieve a directivity value greater than 10 dBi. Imagine increasing the number of patches by the array configuration (2 x 2 and 4 x 4) – what will then be the realized gain? The array arrangement of patches provides a significant boost in realized gain of more than 4 dB (see Figure 16), as well as improved directivity and efficiency. In Figure 15, the total antenna efficiency is always less than the antenna's radiation efficiency. In other words, the radiation efficiency is the same as the total antenna efficiency if there is no loss due to impedance mismatch. As can be seen in Figures 15 and 16, the array configuration of patches significantly improves efficiency, directivity, and realized gain. From the findings listed in Table 4, by examining the parameters at 87.7 GHz (first stage) and 91.5 GHz (second stage)separately, when compared to those of the other frequency bands in the same stage, we deduce that the proposed antenna must be designed to operate in the region of frequencies around 90 GHz, as the high reflection coefficient indicates more radiated power (Figures 4, 9, and 10). On the other hand, the impedance matching is described by the close proximity of the two curves (radiation and total efficiency) around 90 GHz for both stages. The wide realized bandwidth (15.83 GHz), especially at 91.5 GHz, is due to the adopted approach of altering the form of the patch or the main feed line width during the design optimization in the second stage. This bandwidth was 1.4 times bigger than that realized in the first stage at 87.7 GHz.

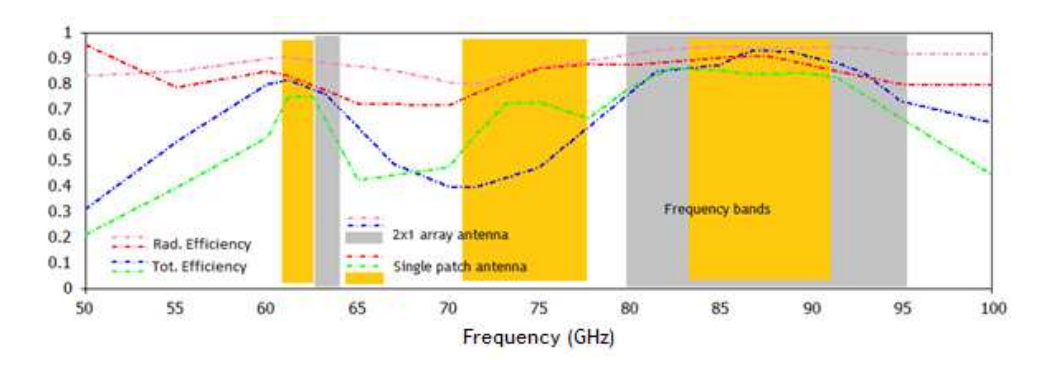


Figure 15 Radiation efficiency and total efficiency for the single-patch and 2×1 array antennas as a function of frequency.

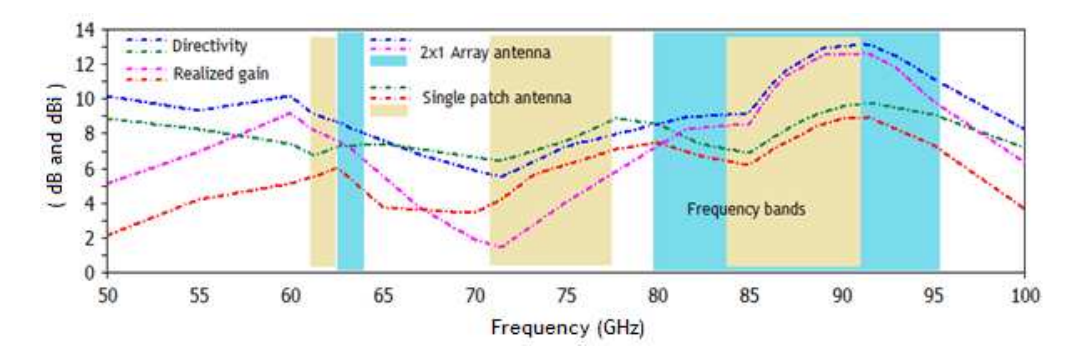


Figure 16 Realized gain and directivity as a function of frequency for the single patch and 2×1 array antennas.

The increase in gain and bandwidth was mostly attributable to the optimal values of several design factors. As previously stated in relation to the part that significantly affects the radiation characteristics, i.e., gain and efficiency, in this context it is necessary to investigate the effects of important design factors on the resonance performance of the proposed antenna. Figures 17(a) and(b) depict the reasoning behind the use of stubs and elliptic-shaped sides in greater detail. Figure 17 shows that the elliptic-shaped lateral edges on both sides of the patch are the primary factors in antenna performance or radiating power; this is translated by the amount of current present on the surface of the patch. As can be observed, current flows are more dominant and concentrated near the stated spots. In addition to the major role of the elliptic-shaped lateral edges in radiating at 87.7 GHz, 61.3 GHz, and 63.2 GHz, the horizontal stubs in the front and back of the patch at 91.5 GHz, 87.7 GHz, and 73.25 GHz, as shown in Figures 17(a) and (b), also contribute to radiating, but a little less.

The stubs are important in the proposed antenna's multiband behavior, as they perturb the current distribution on the patch and change the coupling between the patch and the ground plane; they also create additional current paths that change the direction of the surface current flow along the radiating patch. They have the role of giving the antenna multiband behavior and improving the bandwidth, as mentioned in the introduction. When we observe the scale of the current flow, we find that the current density at the level of the antenna with a single patch is higher than that of the 2 x 1 array antenna. This is due to the presence of the power divider feed network; on the other hand, the volume of radiation increases, which confirms the advantage of using an array configuration.

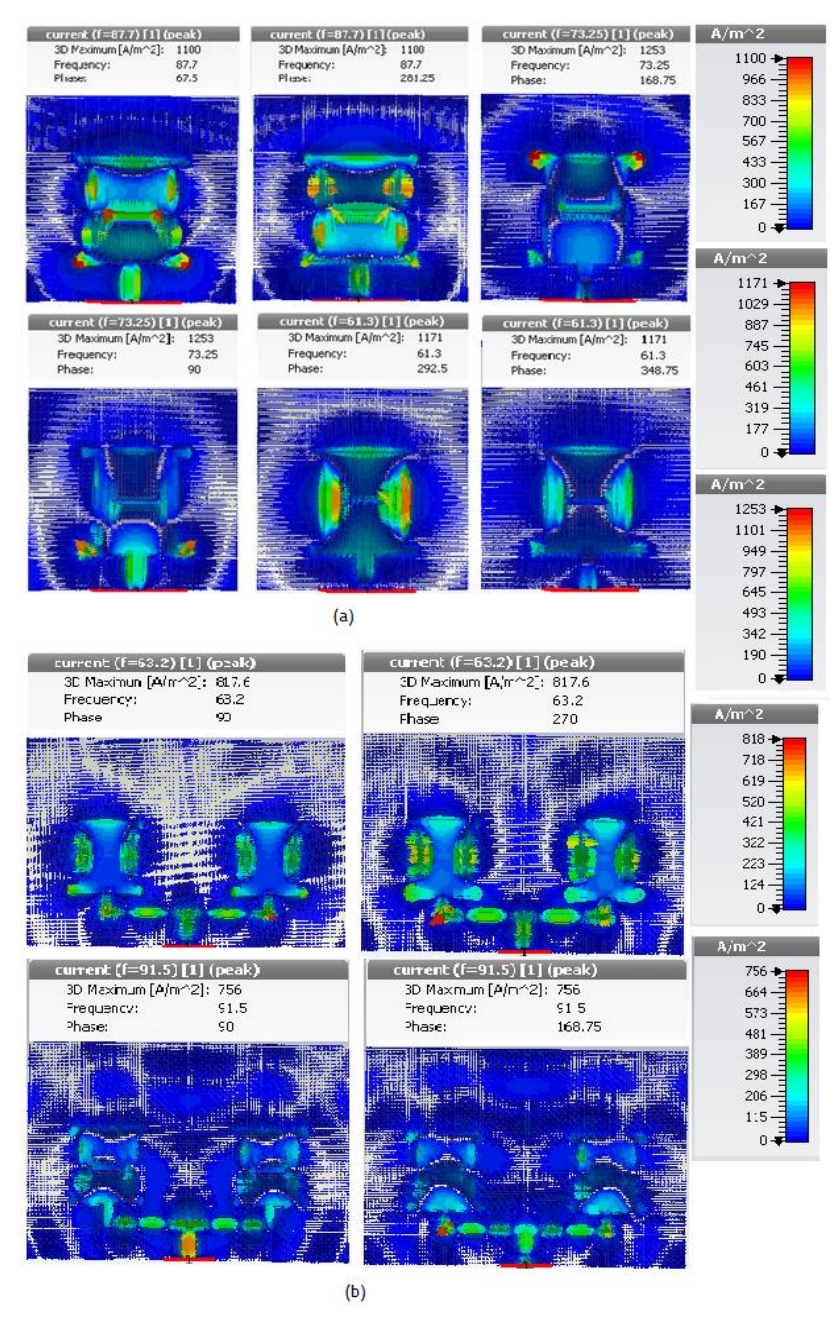


Figure 17 Current density with the (a) single-patch and(b) 2×1 array antenna.

 Table 4
 Simulated results comparison.

Design	Resonant Frequency (GHz)	Realized Gain (dB)	S11(dB)	BW (GHz)	Radiation Efficiency%	Directivity (dBi)
Single patch	61.3	5.55	-20	1.66	83.2	6.75
	73.25	5.67	-17	6.13	81	7.05
	87.7	7.92	-27	6.47	91	8.67
2 x 1	63.2	7.3	-21.18	1.33	88	8.38
element array	91.5	12.56	-47.52	15.83	94	13.11

To assess the performance of the proposed 1×2 array antenna, we compared it to some recent works covering a wide range of frequency bands. Table 5 presents this comparison. In addition to its small size and simple

manufacturing, the proposed antenna performs better than the other works in terms of realized gain and return loss. Except for [58], its considerable bandwidth enables it to be competitive in terms of bandwidth. The proposed antenna is suitable for many millimeter-wave wireless applications because of the aforementioned characteristics.

Compared Work	Resonant Freq (GHz)	Realized Gain (dB)	S11(dB)	BW (GHz)	Tot and Rad Efficiency %	Size (mm²) Type	Design Complexity
[56]	60.08	7.12	-26.08	3.52	75.5 tot.eff	10.7 × 4 Single patch	Relatively easy
[57]	60	11.4	-12.23	1	_	33.5 × 8 Single patch	Relatively complex
[47]	62.5	11.2	-7.36	≤ 0.5	96. rad.eff	33.5 × 8 Array 2 × 1	Complex
[43]	61	10.1	-38	10	-	40 × 10 Array 2 × 1	Complex
[58]	60 80	7.92 7.18	-16 -18	42 20	95 rad.eff 85 rad.eff	15.5 × 6 Array 2 × 1	Easy
[59]	60	8.2	-47	6	_	14 × 13 Array 2 × 2	Complex
[60]	77 65	11.5 7	-25 -28	2 1	_ _	5.2 × 19 Array 8 × 2	Complex
[61]	54	12.1	-18	1.3	93 rad.eff	24 × 6 Array 4 × 1	Easy
This work	63.2 91.5	7.33 12.56	-21.18 -41.52	1.33 15.83	80 Tot.eff 88 Tot.eff	9 × 14 Array 2 × 1	Easy

Table 5 Comparison with some recent works.

Conclusion

The basic realities represented by bandwidth shortages at lower frequencies, high-speed communication needs, and the unimaginable data amounts of several devices are the reasons that led us to present this work. The paper proposed a miniaturized 2 x 1 patch array antenna for millimeter-wave applications operating at the 91.5 GHz and 63.2 GHz bands. The proposed antenna has a high gain of 12.56 dB with a radiation efficiency of 94 percent, an ultra-wide bandwidth of 15.83 GHz, and a return loss of -47.52 dB in the 91.5 GHz frequency band. Few such incredibly tiny, innovative dual-band antennas with remarkable results have been published in the literature to date. The next task is to design 2 x 2 and 4 x 4 antenna arrays, with which we expect to further enhance bandwidth, efficiency, and gain.

References

- [1] Sharma, N., Gautam, A.K. &Kanaujia, B.K., *Circularly Polarized Square Slot Microstrip Antenna for RFID Applications*, International Journal of Microwave and Wireless Technologies, **8**(8), pp. 1237- 1242, Dec. 2016.
- [2] Zaid, J., Farahani, M.M. & Denidni, T.A., *Magneto-Dielectric Substrate-Based Microstrip antenna for RFID Applications, IET Microwaves*, Antennas & Propagation, **11**(10), pp. 1389 -1392, Jul.2017. doi:10.1049/ietmap.2016.0931.
- [3] Nguyen, C.C., Bui, M.D., Nguyen, N.K. & Nguyen, V.T., *Optimal Design of V-Shaped Fin Heat Sink for Active Antenna Unit of 5G Base Station*, Journal of Engineering and Technological Sciences, **54**(3), pp. 568–579, Jan. 2022. doi: 10.5614/j.eng.technol.sci.2022.54.3.9
- [4] Agrawal, T. & Srivastava, S., *Compact MIMO Antenna for Multiband Mobile Applications, Journal of Microwaves*, Optoelectronics and Electromagnetic Applications, **16**(2), pp. 5542-552, Jun. 2017. doi: 10.1590/2179-10742017v16i2899.
- [5] Hmamou, A., El Ghzaoui, M., Foshi, J. & Mestoui, J., *Experimental and Theoretical Analysis of Throughput of MIMO PLC Network*, Journal of Engineering and Technological Sciences, **54**(3), pp. 548-567, Nov. 2022. doi: 10.5614/j.eng.technol.sci.2022.54.3.8

- [6] Paul, L.C., Hosain, Md. S., Sarker, S., Prio, M.H., Morshed, M. & Sarkar, A.K., *The Effect of Changing Substrate Material and Thickness on the Performance of Inset Feed Microstrip Patch Antenna*, American Journal of Networks and Communications, **4**(3), pp. 54-58, May. 2015.
- [7] Kim, J.H., Ahn, C.H. & Chun, J.C., Bandwidth Enhancement of a Slot Antenna with An Open Stub, Microwave and Optical Technology Letters, **60**(1), pp. 248 -252. Jan. 2018. doi:10.1002/mop.30951.
- [8] Avignon-Meseldzija, E., Lepetit, T., Ferreira, P.M. & Boust, F., Negative Inductance Circuits for Metamaterial Bandwidth Enhancement, EPJ Applied Metamaterials, 4(11), Nov. 2017, doi: 10.1051/epjam/2017009.
- [9] Lee, Y.-H., Cho, S.-Y. & Chung, J.-Y., SNR Enhancement of an Electrically Small Antenna Using a Non-Foster Matching Circuit, Applied Sciences, **10**(13), 4464, 28 Jun. 2020. doi:10.3390/app10134464.
- [10] Alibakhshikenari, M., Virdee, B., Shukla, P., Wang, Y., Azpilicueta, L., Moghadasi, M. N., See, C. H., Elfergani, I., Zebiri, C., Abd-alhameed, R., Huynen, I., Rodriguez, J., Denidni, T. A., Falcone, F. & Limiti, E., Impedance Bandwidth Improvement of a Planar Antenna Based on Metamaterial-Inspired T-Matching Network, IEEE Access, 9, pp. 67916-67927, May. 2021. doi: 10.1109/ACCESS.2021.3076975
- [11] Alibakhshikenari, M., Virdee, B., Shukla, p., See, c. H., Abd Alhameed, R. A., falcone, f. & Limiti, E., Improved Adaptive Impedance Matching for RF Front-End Systems of Wireless Transceivers, Scientific Reports, 10, 14065 Aug. 2020, doi: 10.1038/s41598-020-71056-0
- [12] Alibakhshikenari, M., Virdee, B.S., See, C. H., Abd-Alhameed, R. A., Falcone, F. & Limiti, E., *Impedance Matching Network Based on Metasurface (2-D Metamaterials) for Electrically Small Antennas*, 2020 IEEE International Symposium on Antennas and Propagation and North American Radio Science Meeting (2020 IEEE AP-S/URSI), pp.1953-1954, Montréal, Québec, Canada on 5-10 July. 2020.
- [13] Alibakhshikenari, M., Virdee, B.S., See, C.H., Abd-Alhameed, R.A., Falcone, F. & Limiti, E., *Automated Reconfigurable Antenna Impedance for Optimum Power Transfer*, 2019 IEEE Asia-Pacific Microwave Conference (APMC), Singapore, Singapore, pp. 1461-1463, 2019. doi: 10.1109/APMC46564.2019.9038260
- [14] Alibakhshikenari, M., Virdee, B., See, C.H., Abd-Alhameed, R.A., Falcone, F. & Limiti, E., *Energy Harvesting Circuit with High RF-to-DC Conversion Efficiency*, 2020 IEEE International Symposium on Antennas and Propagation and North American Radio Science Meeting (2020 IEEE AP-S/URSI), pp.1299-1300, Montréal, Québec, Canada on 5-10 July. 2020. doi: 10.1109/IEEECONF35879.2020.93296
- [15] Roy, A.A., Môm, J.M. & Igwue, G.A., Enhancing the Bandwidth of a Microstrip Patch Antenna using Slots Shaped Patch, American Journal of Engineering Research (AJER), 2(9), pp-23-30, Jan. 2013. doi: 10.13140/RG.2.1.2479.7044
- [16] Bhanumathiand, V. & Swathi, S., *Bandwidth Enhanced Microstrip Patch Antenna for UWB Applications*, ICTACT Journal on Microelectronics, 4(4), pp. 669-675, Jan. 2019, doi: 10.21917/ijme.2019.01116.
- [17] Nawale, P.A. & Zope, R.G., *Design and Improvement of Microstrip Patch Antenna Parameters Using Defected Ground Structure*, Int. Journal of Engineering Research and Applications, **4**(6), pp. 123-129, Jun. 2014
- [18] Rahman, M.M., Islam, M.S., Wong, H.Y., Alam, T. & Islam, M.T., *Performance Analysis of a Defected Ground-Structured Antenna Loaded with Stub-Slot for 5G Communication*, Sensors, **19**(11), pp. 2634, Jun. 2019. doi:10.3390/s19112634.
- [19] Muhamad, W.A.W., Ngah, R., Jamlos, M. F., Soh, P.J., Jamlos, M.A. & Lago, H., *Antenna Array Bandwidth Enhancement Using Polymeric Nano-Composite Substrate*, Applied Physics A, **122**(426), pp. 1-9, Mar. 2016, doi: 10.1007/s00339-016-9887-z.
- [20] Peng, Y., Rahman, B.M.F., Wang, X. & Wang, G., *Performance Enhanced Miniaturized and Electrically Tunable Patch Antenna with Patterned Permalloy Based Magneto-Dielectric Substrate*, Journal of Applied Physics, 115(17), 17A505(1-4), Jan. 2014. doi: 10.1063/1.4861203.
- [21] Yang, X.M., Wen, J., Liu, C. R., Liu, X.G. & Cui, T.J., Broadbanding of Circularly Polarized Patch Antenna by Waveguided Magneto-Dielectric Metamaterial, AIP Advances, 5(12), 127134, Dec. 2015. doi:10.1063/1.4939218.
- [22] Tyagi, N., Singh, S. & Sinha, N., Enhancement of Bandwidth in Microstrip Patch Antenna using EBG, International Journal of Computer Applications (IJCA), **92**(15), pp. 27-31, Apr. 2014. doi: 10.5120/16085-5293.
- [23] Kaabal, A., El halaoui, M., ElJaafari, B., Ahyoud, S. & Asselman, A., *Design of EBG Antenna with Multi-*. *Sources Excitation for High Directivity Applications*, Procedia Manufacturing, **22**, pp. 598-604,2018.

- [24] Tamrakar, M. & Kiran, K.U., Bandwidth Enhancing Method Using Tri-Ring Resonator Metamaterial for Small Devices, Microwave and Optical Technology Letters, **61**(2), pp. 1-5, Dec. 2018. doi: 10.1002/mop.31701.
- [25] Patel, S.K. & Argyropoulos, C., Enhanced Bandwidth and Gain of Compact Microstrip Antennas Loaded with Multiple Corrugated Split Ring Resonators, Journal of Electromagnetic Waves and Applications, **30**(7), pp. 945-961, May. 2016. doi: 10.1080/09205071.2016.1167633.
- [26] Annou, A., Berhab, S. & Chebbara, F., *Metamaterial Fractal Defected Ground Structure Concepts Combining for Highly Miniaturized Triple-Band Antenna Design*, Journal of Microwaves, Optoelectronics and Electromagnetic Applications (JMOEA), **19**(4), pp. 522-541, Dec. 2020. doi: 10.1590/2179-10742020v19i4894.
- [27] Kaushal, D. & Shanmuganantham, T., *Parametric Enhancement of a Novel Microstrip Patch Antenna using Circular SRR Loaded Fractal Geometry*, Alexandria Engineering Journal, **57**(4), pp. 2551-2557, Sep. 2017.
- [28] Haran, M., Kumar, G. D., Garvin, A. F. & Ramesh, S., *Hexagonal Microstrip Patch Antenna for Early-Stage Skin Cancer Identification*, Telecommunications and Radio Engineering, **79**(7), pp. 555-566, 2020. doi: 10.1615/TelecomRadEng.v79. i7.20
- [29] Kubacki, R., Czyżewski, M. & Laskowski, D., *Minkowski Island and Crossbar Fractal Microstrip Antennas for Broadband Applications*, Applied Sciences, **8**(3), 334, Feb. 2018. doi: 10.3390/app8030334.
- [30] Baard, C., Liu, Y. & Nikolova, N., *Ultra-Wideband Low-Cost High-Efficiency Cavity-Backed Compound Spiral Antenna*, Electronics, **9**(9), 1399, Aug. 2020. doi:10.3390/electronics9091399.
- [31] Ramesh, S. & Rao, T.R., Dielectric Loaded Exponentially Tapered Slot Antenna Utilizing Substrate Integrated Waveguide Technology for Millimeter Wave Applications, Progress in Electromagnetic Research C, 42, pp. 149-164, 2013. doi:10.2528/pierc13062003.
- [32] Ramesh, S. & Rao, T.R., High Gain Dielectric Loaded Exponentially Tapered Slot Antenna Based on Substrate Integrated Waveguide for V-Band Wireless Communications, Aces Journal, 29(11), Nov. 2014.
- [33] Niu, B. & Tan, J.-H., Bandwidth Enhancement of Low-Profile SIW Cavity Antenna with Bilateral Slots, Electronics Letters, **55**(5), pp. 233-234, Mar. 2019. doi: 10.1049/el.2018.7569.
- [34] Rao, K.P., Vani, R.M. & Humayun, P.V., *Planar Microstrip Patch Antenna Array with Gain Enhancement, Procedia Computer Science*, **143**, pp. 48-57, 2018. doi: 10.1016/j.procs.2018.10. 350.
- [35] Hu, W., Wen, G., Inserra, D., Huang, Y., Li, J. & Chen, Z., A *Circularly Polarized Antenna Array with Gain Enhancement for Long-Range UHF RFID Systems*, Electronics, **8**(4), 400, Apr. 2019. doi: 10.3390/electronics8040400.
- [36] Alibakhshikenari, M., Babaeian, F., Virdee, B.S., Aïssa, S., Azpilicueta, L., See, C.H., Althuwayb, A.A., Huynen, I., Abd-Alhameed, R., Falcone, F. & Limiti, E., A Comprehensive Survey on Various Decoupling Mechanisms with Focus on Metamaterial and Metasurface Principles Applicable to SAR and MIMO Antenna Systems, IEEE Access, 8, pp. 192965-193004, Oct. 2020. doi: 10.1109/ACCESS.2020.3032826
- [37] Alibakhshikenari, M., Virdee, B.S. & Limiti, E., Study on Isolation and Radiation Behaviours of a 34×34 Array-Antennas Based on SIW and Metasurface Properties for Applications in Terahertz Band Over 125-300 GHz, Optik, International Journal for Light and Electron Optics, **206**, 163222, Mar. 2020.
- [38] Alibakhshikenari, M., Virdee, B.S., Shukla, P., See, C.H., Abd-Alhameed, R., Khalily, M., Falcone, F., Limiti, E., Quazzane, K. & Parchin, N., *Isolation Enhancement of Densely Packed Array Antennas with Periodic MTM-Photonic Bandgap for SAR and MIMO Systems*, IET Microwaves, Antennas & Propagation, **14**(3), pp. 183 188, Feb. 2020.
- [39] Alibakhshikenari, M., Virdee, B.S., See, C.H., Abd-Alhameed, R.A., Falcone, F. & Limiti, E., Surface Wave Reduction in Antenna Arrays Using Metasurface Inclusion for MIMO and SAR Systems, Radio Science, 54(11), pp. 1067–1075, Nov. 2019.
- [40] Alibakhshikenari, M., Khalily, M., Virdee, B.S., See, C.H., Abd-Alhameed, R.A. & Limiti, E., *Mutual-Coupling Isolation Using Embedded Metamaterial EM Bandgap Decoupling Slab for Densely Packed Array Antennas*, IEEE Access, **7**, pp. 5182–51840, Apr. 2019. doi: 10.1109/ACCESS.2019.2909950.
- [41] Alibakhshikenari, M., Khalily, M., Virdee, B.S., See, C.H., Abd-Alhameed, R.A. & Limiti, E., *Mutual Coupling Suppression Between Two Closely Placed Microstrip Patches Using EM-Bandgap Metamaterial Fractal Loading*, IEEE Access, **7**, pp. 23606 23614, Feb. 2019. doi: 10.1109/ACCESS.2019.2899326.
- [42] Alibakhshikenari, M., Virdee, B.S., Azpilicueta, L., Moghadasi, M.N., Akinsolu, M.O., See, C., Liu, B., Abd-Alhameed, R.A., Falcone, F., Huynen, I., Denidni, T.A. & Limiti, E., *A Comprehensive Survey of Metamaterial Transmission-Line Based Antennas: Design, Challenges, and Applications*, IEEE Access, **8**, pp. 144778-144808, Aug. 2020. doi:10.1109/ACCESS.2020.3013698.

- [43] Alibakhshikenari, M., Virdee, B.S., See, C.H., Abd-Alhameed, R.A., Falcone, F. & Limiti, E., High-Isolation Leaky-Wave Array Antenna Based on CRLH Metamaterial Implemented on SIW with ±300 Frequency Beam-Scanning Capability at Millimeter-Waves, Electronics, 8(6), 642, Jun. 2019. doi: 10.3390/electronics806064.
- [44] Alibakhshikenari, M., Virdee, B.S., See, C.H., Abd-Alhameed, R.A., Falcone, F. & Limiti, E., *Super-Wide Impedance Bandwidth Planar Antenna for Microwave and Millimeter-Wave Applications*, Sensors, **19**(10), 2306, 9 pages, May 2019, doi: 10.3390/s19102306.
- [45] Alibakhshikenari, M., Virdee, B.S., Khalily, M., Shukla, P.R., See, C.H., Abd-Alhameed, R.A., Falcone, F. & Limiti, E., *Beam-Scanning Leaky-Wave Antenna Based on CRLH-Metamaterial for Millimeter-Wave Applications*, IET Microwaves, Antennas & Propagation, **13**(8), pp. 1129-1133, Mar. 2019. doi: 10.1049/iet-map.2018.5101.
- [46] Alibakhshikenari, M., Virdee, B.S., AbdulAli & Limiti, E., A Novel Monofilar-Archimedean Metamaterial Inspired Leaky-Wave Antenna For Scanning Application For Passive Radar Systems, Microwave and Optical Technology Letters, 60(8), pp. 2055–2060, Jun. 2018.
- [47] Alibakhshikenari, M., Virdee, B. S., AbdulAli & Limiti, E., Miniaturized Planar-Patch Antenna Based on Metamaterial L-shaped Unit-Cells for Broadband Portable Microwave Devices and Multiband Wireless Communication Systems, IET Microwaves, Antennas & Propagation, 12(7), pp. 1080 -1086, Jun. 2018.
- [48] Alibakhshikenari, M., Virdee, B. S., AbdulAli & Limiti, E., *Compact Single Layer Travelling-Wave Antenna Design Using Metamaterial Transmission-Lines*, Radio Science, **52**(12), pp. 1510-1521, Dec. 2017. doi: 10.1002/2017RS006313.
- [49] Alibakhshikenari, M., Ali, E.M., Soruri, M., Dalarsson, M., Moghadasi, M.N., Virdee, B.S., Stefanovic, C., Dabrowska, A.P., Koziel, S., Szczepanski, S. & Limiti, E., A Comprehensive Survey on Antennas on-Chip Based on Metamaterial, Metasurface, and Substrate Integrated Waveguide Principles for Millimeter-Waves and Terahertz Integrated Circuits and Systems, IEEE Access, 10, pp. 3668-3692, Jan. 2022. doi: 10.1109/ACCESS.2021.3140156
- [50] Alibakhshikenari, M., Virdee, B.S., Althuwayb, A.A., Mariyanayagam, D. & Limiti, E., Compact and Low-Profile On-Chip Antenna Using Underside Electromagnetic Coupling Mechanism for Terahertz Front-End Transceivers, Electronics, 10(11), 1264, May. 2021, doi: 10.3390/electronics10111264.
- [51] Althuwayb, A.A., Alibakhshikenari, M., Virdee, B.S., Benetatos, H., Falcone, F. & Limiti, E., *Antenna on Chip (AoC) Design Using Metasurface and SIW Technologies for THz Wireless Applications*, Electronics, **10**(9), 1120, May. 2021. doi: 10.3390/electronics10091120.
- [52] Alibakhshikenari, M., Virdee, B.S., Althuwayb, A.A., Sonia, A., See, C.H., Abd-Alhameed, R.A., Falcone, F. & Limiti, E., Study on on-Chip Antenna Design Based on Metamaterial-Inspired and Substrate-Integrated Waveguide Properties for Millimetre-Wave and THz Integrated-Circuit Applications, Journal of Infrared, Millimeter, and Terahertz Waves, 42, pp. 17-28, Jan. 2021. doi: 10.1007/s10762-020-00753-8.
- [53] Alibakhshikenari, M., Virdee, B. S., Khalily, M., See, C. H., Abd-Alhameed, R. A., Falcone, F., Denidni, T. A. & Limiti, E., *High-Gain On-Chip Antenna Design on Silicon Layer with Aperture Excitation for Terahertz Applications*, IEEE Antennas and Wireless Propagation Letters, **19**(9), pp. 1576-1580, Sept. 2020. doi: 10.1109/lawp.2020.3010865.
- [54] Ghattas, A.S.W., Saad, A.A.R. & Khaled, E.E.M., *Compact Patch Antenna Array for 60 GHz Millimeter-Wave Broadband Applications*, Wireless Personal Communications, **114**(1), pp. 2821-2839, Oct. 2020, doi: 10.1007/s11277-020-07505-w.
- [55] Fagiani, A., Vogel, M. & Cerqueira, S.Jr.A., *Material Characterization and Propagation Analysis of mm-Waves Indoor Networks*, Journal of Microwaves, Optoelectronics and Electromagnetic Applications (JMOEA), **17**(4), pp. 628-637, Dec. 2018. doi:10.1590/2179-10742018v17i41548.
- [56] Kumar, M.N. & Shanmuganantham, T., *E-Shaped Slot Antenna Backed with Substrate Integrated Waveguide Cavity for 60GHz Applications*, Proc. IEEE Conference on Emerging Devices and Smart Systems (ICEDSS), 3-4 March. 2017, Mahendra Engineering College, Tamilnadu, India, 2017. doi: 10.1109/icedss.2017.8073651.
- [57] Ramesh, S. & Rao, T.R., Indoor Channel Characterization Studies For V-Band Gigabit Wireless Communications Using Dielectric-Loaded Exponentially Tapered Slot Antenna, International Journal of Microwave and Wireless Technologies, 8(8), pp. 1243-1251, 2015. doi: 10.1017/s1759078715000781.

- [58] Ullah, R., Ullah, S., Umar, S. M., Ullah, R. & Babar, K., Design and Modeling of a 28/38/60/70/80 GHz Antenna for Fifth Generation 5G Mobile and Millimeter Wave Applications, Proc. of the 1st International Conference on Electrical, Communication and Computer Engineering (ICECCE), Swat, Pakistan, July. 2019. doi: 10.1109/ICECCE47252.2019.8940640.
- [59] Ullah, S., Yeo, W.H., Kim, H. & Yoo, H., Development Of 60-Ghz Millimeter Wave, Electromagnetic Bandgap Ground Planes for Multiple-Input Multiple-Output Antenna Applications, Scientific Reports, 10(8541), 2020. doi: 10.1038/s41598-020-65622-9.
- [60] Kim, S., Rida, A., Lakafosis, V., Nikolaou, S. & Tentzeris, M.M., 77-Ghz Mm wave Antenna Array on Liquid Crystal Polymer for Automotive Radar and RF Front-End Module, ETRI Journal, 41(2), pp. 262-269, Jan. 2019. doi: 10.4218/etrij.2018-0163.
- [61] Imran, D., Farooqi, M.M., Khattak, M. I., Ullah, Z., Khan, M.I., Khattak, M.A. & Dar, H., *Millimeter Wave Micro strip Patch Antenna for 5G Mobile Communication*, International Conference on Engineering and Emerging Technologies (ICEET), Lahore, Pakistan, Feb. 2018. doi: 10.1109/ICEET1.2018.8338623.